

Internal Excitation in the Products of Nucleophilic Substitution from the Dissociation of Metastable Ion Complexes

Susan T. Graul,^{*,‡} Catherine J. Carpenter,[†] John E. Bushnell,[†]
Petra A. M. van Koppen,[†] and Michael T. Bowers^{*,‡}

Contribution from the Departments of Chemistry, Carnegie Mellon University, 4400 Fifth Avenue, Pittsburgh, Pennsylvania 15213, and University of California, Santa Barbara, California 93106

Received September 2, 1997

Abstract: The relative kinetic energy distributions for the products of the dissociation of four metastable gas-phase ion clusters have been analyzed by means of ion kinetic energy spectroscopy, and the results modeled using statistical phase space theory. The systems studied represent reaction intermediates in bimolecular nucleophilic substitutions (S_N2). These studies build on previous investigations that demonstrated vibrational excitation in the products of the substitution reactions of halide ions with methyl halides.¹ The present studies explore the effects of molecular structure, reaction exothermicity, and nucleophile and leaving group variation. The experimental kinetic energy distributions are compared with theoretical distributions calculated for statistical partitioning of energy among internal modes and relative kinetic energy of the products. In each reaction, the calculated distributions agree with the experimental distributions only if a significant fraction of the energy released in the exothermic reactions is assumed to be unavailable for randomization in the dissociation. The results suggest that the products of these S_N2 reactions are internally excited.

Introduction

Bimolecular nucleophilic substitution (S_N2) reactions are some of the most widely studied reactions in solution,² and have been the object of a number of gas-phase studies as well.^{1–8} In this latter case, statistical theories, such as RRKM and phase space theory,^{9–15} have often been invoked as models for the

kinetics and dynamics of these reactions.^{16–20} A major assumption in these statistical theories is that energy is rapidly randomized due to strong coupling among the modes of the reacting molecules. As a result, properties such as reaction rates and product energy deposition can be predicted by using only densities of states of the reactants, products, and transitions states.

Recently, however, there has been theoretical and experimental evidence that some S_N2 reactions may not behave statistically.^{1,21–26} For example, quantum dynamical and reaction path Hamiltonian calculations show nonstatistical behavior for $X^- + CH_3F \rightarrow F^- + CH_3X$ ($X = H, F, OH$), including formation of vibrationally excited products.^{23,24} Hase and co-workers have performed trajectory calculations for the reactions $^aCl^- + CH_3^bCl \rightarrow ^bCl^- + CH_3^aCl$ and $Cl^- + CH_3Br \rightarrow Br^- +$

[‡] Carnegie Mellon University.

[†] University of California.

(1) (a) Graul, S. T.; Bowers, M. T. *J. Am. Chem. Soc.* **1991**, *113*, 9696–9697. (b) Graul, S. T.; Bowers, M. T. *J. Am. Chem. Soc.* **1994**, *116*, 3875–3883.

(2) Shaik, S. S.; Schlegel, H. B.; Wolfe, S. *Theoretical Aspects of Physical Organic Chemistry. The S_N2 Mechanism*; Wiley-Interscience: New York, 1992.

(3) (a) Bohme, D. K.; Mackay, G. I.; Payzant, J. D. *J. Am. Chem. Soc.* **1974**, *96*, 4027–4028. (b) Tanaka, K.; Mackay, G. I.; Payzant, J. D.; Bohme, D. K. *Can. J. Chem.* **1976**, *54*, 1643–1659.

(4) (a) Lieder, C. A.; Brauman, J. I. *J. Am. Chem. Soc.* **1974**, *96*, 4029–4030. (b) Brauman, J. I.; Olmstead, W. N.; Lieder, C. A. *J. Am. Chem. Soc.* **1974**, *96*, 4030–4031. (c) Olmstead, W. N.; Brauman, J. I. *J. Am. Chem. Soc.* **1977**, *99*, 4219–4228. (d) Asubiojo, O. I.; Brauman, J. I. *J. Am. Chem. Soc.* **1979**, *101*, 3715–3724. (e) Pellerite, M. J.; Brauman, J. I. *J. Am. Chem. Soc.* **1980**, *102*, 5993–5999. (f) Wilbur, J. L.; Wladkowski, B. D.; Brauman, J. I. *J. Am. Chem. Soc.* **1993**, *115*, 10823–10829. (g) Wladkowski, B. D.; Wilbur, J. L.; Brauman, J. I. *J. Am. Chem. Soc.* **1994**, *116*, 2471–2480.

(5) (a) DePuy, C. H.; Gronert, S.; Mullin, A.; Bierbaum, V. M. *J. Am. Chem. Soc.* **1990**, *112*, 8650–8655. (b) Gronert, S.; DePuy, C. H.; Bierbaum, V. M. *J. Am. Chem. Soc.* **1991**, *113*, 4009–4010.

(6) Cyr, D. M.; Posey, L. A.; Bishea, G. A.; Han, C.-C.; Johnson, M. A. *J. Am. Chem. Soc.* **1991**, *113*, 9697–9699.

(7) Cyr, D. M.; Baily, C. G.; Serxner, D.; Scarton, M. G.; Johnson, M. A. *J. Chem. Phys.* **1994**, *101*, 10507–10520.

(8) Li, C.; Ross, P.; Szulejko, J. E.; McMahon, T. B. *J. Am. Chem. Soc.* **1996**, *118*, 9360–9367.

(9) Forst, W. *Theory of Unimolecular Reactions*; Academic Press: New York, 1973.

(10) Robinson, P. J.; Holbrook, K. A. *Unimolecular Reactions*; Wiley-Interscience: New York, 1972.

(11) Pechukas, P. In *Dynamics of Molecular Collisions, Part B*; Miller, W. H., Ed.; Plenum Press: New York, 1976.

(12) Chesnavich, W. J.; Bowers, M. T. In *Gas-Phase Ion Chemistry*; Bowers, M. T., Ed.; Academic Press: New York, 1979; Vol. 1, pp 119–151.

(13) Pechukas, P.; Light, J. C.; Rankin, C. J. *J. Chem. Phys.* **1966**, *44*, 794–805.

(14) Nikitan, E. *Theor. Exp. Chem. (Engl. Transl.)* **1965**, *1*, 285.

(15) (a) Chesnavich, W. J.; Bowers, M. T. *J. Am. Chem. Soc.* **1976**, *98*, 8301–8309. (b) Chesnavich, W. J.; Bowers, M. T. *J. Chem. Phys.* **1978**, *68*, 901–910. (c) Chesnavich, W. J.; Bowers, M. T. *Prog. React. Kinet.* **1982**, *11*, 137–267.

(16) (a) Dodd, J. A.; Brauman, J. I. *J. Phys. Chem.* **1986**, *90*, 3559–3562. (b) Wladkowski, B. D.; Lim, K. F.; Allen, W. D.; Brauman, J. I. *J. Am. Chem. Soc.* **1992**, *114*, 9136–9153.

(17) Pellerite, M. J.; Brauman, J. I. *J. Am. Chem. Soc.* **1983**, *105*, 2672–2680.

(18) Caldwell, G.; Magnera, T. F.; Kebarle, P. *J. Am. Chem. Soc.* **1984**, *106*, 959–966.

(19) Barlow, S. E.; Van Doren, J. M.; Bierbaum, V. M. *J. Am. Chem. Soc.* **1988**, *110*, 7240–7242.

(20) Viggiano, A. A.; Morris, R. A.; Su, T.; Wladkowski, B. D.; Craig, S. L.; Zhong, M.; Brauman, J. I. *J. Am. Chem. Soc.* **1994**, *116*, 2213–2214.

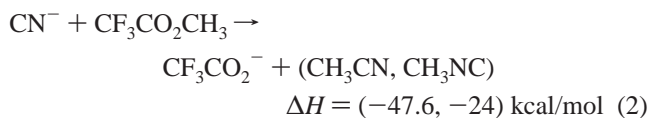
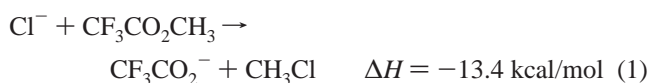
(21) (a) Bergsma, J. P.; Gertner, B. J.; Wilson, K. R.; Hynes, J. T. *J. Chem. Phys.* **1987**, *86*, 1356–1376. (b) Gertner, B. J.; Whitnel, R. M.; Wilson, K. R.; Hynes, J. T. *J. Am. Chem. Soc.* **1991**, *113*, 74–87.

CH_3Cl .²² The results are indicative of nonstatistical dynamics, including vibrational state-specific rate enhancement, multiple crossings of the transition state (TS) dividing surface, and nonstatistical product energy distributions. Reaction path Hamiltonian calculations for the $\text{Cl}^- + \text{CH}_3\text{Br}$ reaction indicate weak coupling between the intramolecular and intermolecular modes of the ion-dipole complex, which inhibits rapid energy randomization.²⁷

Experimental evidence also supports the view that some $\text{S}_{\text{N}}2$ reactions may not behave statistically. Viggiano et al. have found that the rate constant for $\text{Cl}^- + \text{CH}_3\text{Br} \rightarrow \text{Br}^- + \text{CH}_3\text{Cl}$ does not depend on the internal temperature of CH_3Br between 207 and 564 K,²⁵ whereas RRKM theory predicts a positive temperature dependence over the same temperature range.²⁸ The rate constant for ${}^a\text{Cl}^- + {}^b\text{ClCH}_2\text{CN} \rightarrow {}^b\text{Cl}^- + {}^a\text{ClCH}_2\text{CN}$ has also been measured versus ClCH_2CN temperature.²⁰ In contrast to what they observed for the $\text{Cl}^- + \text{CH}_3\text{Br}$ reaction, Viggiano et al. found that the rate constant does depend on the internal energy of the neutral reactant, and obtained reasonable agreement for both the relative kinetic energy dependence and temperature dependence with RRKM theory. They suggest the statistical behavior of the $\text{Cl}^- + \text{ClCH}_2\text{CN}$ reaction is due to the longer lifetime of the ion-dipole complex, which allows for statistical energy exchange.

In addition to the kinetics studies, possible nonstatistical behavior in $\text{S}_{\text{N}}2$ reactions has been investigated by measuring the energy partitioned into the relative translation of the products. In an experiment with kinetic energy-ion cyclotron resonance (KE-ICR) spectroscopy, the CH_3F product of the $\text{S}_{\text{N}}2$ reaction $\text{F}^- + \text{CH}_3\text{Cl} \rightarrow \text{Cl}^- + \text{CH}_3\text{F}$ was found to be vibrationally cold compared to the statistical prediction.²⁶ In contrast, kinetic energy release distribution (KERD) experiments on the $\text{S}_{\text{N}}2$ reactions $\text{X}^- + \text{CH}_3\text{Y} \rightarrow \text{Y}^- + \text{CH}_3\text{X}$ ($\text{X} = \text{Cl}, \text{Br}$; $\text{Y} = \text{Br}, \text{I}$) show, in all cases, that the products are internally excited relative to statistical predictions.¹

In this paper we expand the range of $\text{S}_{\text{N}}2$ reactions studied to include the following.²⁹



(22) (a) Vande Linde, S. R.; Hase, W. L. *J. Am. Chem. Soc.* **1989**, *111*, 2349–2351. (b) Vande Linde, S. R.; Hase, W. L. *J. Phys. Chem.* **1990**, *94*, 6148–6150. (c) Vande Linde, S. R.; Hase, W. L. *J. Chem. Phys.* **1990**, *93*, 7962–7980. (d) Cho, Y. J.; Vande Linde, S. R.; Zhu, L.; Hase, W. L. *J. Chem. Phys.* **1992**, *96*, 8275–8287. (e) Hase, W. L.; Cho, Y. J. *J. Chem. Phys.* **1993**, *98*, 8626–8639. (f) Wang, H.; Peslherbe, G. H.; Hase, W. L. *J. Am. Chem. Soc.* **1994**, *116*, 9644–9651. (g) Peslherbe, G. H.; Wang, H.; Hase, W. L. *J. Chem. Phys.* **1995**, *102*, 5626–5635.

(23) Basilevsky, M. V.; Ryaboy, V. M. *Chem. Phys. Lett.* **1986**, *129*, 71–75.

(24) Ryaboy, V. M. *Chem. Phys. Lett.* **1989**, *159*, 371–375.

(25) Viggiano, A. A.; Morris, R. A.; Paschekewitz, J. S.; Paulson, J. F. *J. Am. Chem. Soc.* **1992**, *114*, 10477–10482.

(26) VanOrden, S. L.; Pope, R. M.; Buckner, S. W. *Org. Mass Spectrom.* **1991**, *26*, 1003–1007.

(27) Wang, H.; Hase, W. L. *Chem. Phys.* **1996**, *212*, 247–258.

(28) Wang, H.; Hase, W. L. *J. Am. Chem. Soc.* **1995**, *117*, 9347–9356.

(29) Lias, S. G.; Bartmess, J. E.; Liebman, J. F.; Holmes, J. L.; Levin, R. D.; Mallard, W. G. *J. Phys. Chem. Ref. Data* **1988**, *17*, Suppl. 1.



This set of reactions allows us to explore the effects of molecular structure of the neutral reactant, the strength of the nucleophile, overall reaction exothermicity, and the effects of substitution at the inverting carbon center. The experimental approach taken involves generating an ion-molecule complex of each pair of reactants in eqs 1–4 and analyzing the dissociation of this complex. Experimental KERDs are reported and compared with statistical phase space theory predictions to obtain deeper insight into dynamics of the $\text{S}_{\text{N}}2$ reaction.

Experimental Section

These experiments were carried out in a reverse-geometry double-focusing sector mass spectrometer (V.G. ZAB-2F) with a temperature- and pressure-variable ion source. The Cl^- , F^- , and CN^- reactant ions were generated by dissociative electron attachment to CCl_4 , CH_3F , and HCN , respectively. The adduct species were then formed by associative collisions with $\text{CF}_3\text{CO}_2\text{CH}_3$, $\text{CH}_3\text{OC}_6\text{H}_5$, or $\text{C}_2\text{H}_5\text{I}$ with the neutral gas pressure maintained as low as possible to minimize stabilization by secondary collisions. The neutral gas pressures were typically 20–40 mTorr and the source temperature approximately 270–300 K. Under these conditions, the collision frequencies for these reactants are approximately 10^5 – 10^6 s^{-1} , corresponding to 1 to 50 collisions for typical source residence times.

The adduct ions were accelerated into the magnetic sector for mass selection. The adduct ion beam was focused such that its energy spread in an ion kinetic energy scan was about 2 eV fwhm for a typical beam energy of 8010 eV. Product ions resulting from dissociation of metastable³⁰ adduct ions in the field-free region between the magnetic and electrostatic sectors were energy analyzed in the electrostatic sector. The flight time from the ion source to the second field-free region of the instrument is about 10^{-5} s , which means that the metastable dissociation experiments probe the reactions of adduct ions with lifetimes of about 10 μs . Kinetic energy release distributions were derived from the laboratory-energy-analyzed product ion peak shape by a method described previously.³¹ The metastable experiments were repeated several times to verify reproducibility. To ensure that collisional effects were not contributing to the metastable peak shapes, collisional activation studies were carried out by leaking helium gas into the collision cell located in the second field-free region. This experimental configuration does not allow the direct measurement of metastable dissociation rate constants, so only metastable branching ratios were measured.

For theoretical modeling of these reactions, experimental heats of formation and spectroscopic data were used where available. When such data were not available or were incomplete, the molecular and ionic species required for the modeling were studied theoretically with ab initio molecular orbital theory to obtain the energetic and spectroscopic parameters needed. The ab initio calculations were performed with the Gaussian 92 suite of programs.³²

Rate coefficients for the bimolecular reactions have been measured by Olmstead and Brauman⁴ and Grabowski and Owusu.³³ These

(30) Cooks, R. G.; Beynon, J. H.; Caprioli, R. M.; Lester, G. R. *Metastable Ions*; Elsevier: Amsterdam, 1973.

(31) Jarrold, M. F.; Illies, A. J.; Kerchner, N. J.; Wagner-Redeker, W.; Bowers, M. T.; Mandich, M. L.; Beauchamp, J. L. *J. Phys. Chem.* **1983**, *87*, 2213–2221.

(32) *Gaussian 92*, Revision A.; Frisch, M. J.; Trucks, G. W.; Head-Gordon, M.; Gill, P. M. W.; Wong, M. W.; Foresman, J. B.; Johnson, B. G.; Schlegel, H. B.; Robb, M. A.; Replogle, E. S.; Gomperts, R.; Andres, J. L.; Raghavachari, K.; Binkley, J. S.; Gonzalez, E.; Martin, R. L.; Fox, D. J.; DeFrees, D. J.; Baker, J.; Stewart, J. J. P.; Pople, J. A. *Gaussian, Inc.*: Pittsburgh, PA, 1992.

(33) Grabowski, J. J.; Owusu, D. Private communication.

Table 1. Branching Ratios and Average Kinetic Energy Releases for Metastable and Collisionally Activated Dissociation of $\text{Cl}^-(\text{CF}_3\text{CO}_2\text{CH}_3)$, $\text{CN}^-(\text{CF}_3\text{CO}_2\text{CH}_3)$, $\text{F}^-(\text{CH}_3\text{OC}_6\text{H}_5)$, and $\text{Cl}^-(\text{CH}_3\text{CH}_2\text{I})$

complex	product ion	metastable		collisionally activated	
		ratio, %	$\langle E_i \rangle$, meV	ratio, %	$\langle E_i \rangle^a$, meV
$\text{Cl}^-(\text{CF}_3\text{CO}_2\text{CH}_3)$	Cl^-	4	22 ± 6	80	68
	CF_3CO_2^-	96	38 ± 1	20	67
$\text{CN}^-(\text{CF}_3\text{CO}_2\text{CH}_3)$	CN^-	2	29 ± 10	90	68
	CF_3CO_2^-	98	66 ± 3	10	73
$\text{F}^-(\text{CH}_3\text{OC}_6\text{H}_5)$	F^-	5	59 ± 5	60	68
	$\text{C}_6\text{H}_5\text{O}^-$	95	60 ± 2	40	77
$\text{Cl}^-(\text{CH}_3\text{CH}_2\text{I})$	Cl^-	$<2^b$		25	68
	I^-	>98	46 ± 1	75	66

^a Error bars for CAD average kinetic energy release measurements: ± 4 meV. ^b Product not detected; branching ratio is the upper limit.

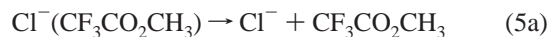
kinetics are modeled with statistical phase space theory, to estimate the energies of the substitution transition state. These values were then used in the statistical phase space models for the kinetic energy release distributions (KERDs). Internal excitation in the products was modeled by calculating a series of KERDs assuming between 0 and 100% of the energy released was unavailable for randomization in the product orbiting transition state. Details of the statistical phase space model are given in the Appendix and the parameters used are available as Supporting Information.

Results

The metastable adduct species are represented in this paper as the reactant complexes $\text{X}^-(\text{RY})$ formed by simple association reactions of $\text{X}^- + \text{RY}$. As will be seen, both the experimental results and the phase space theoretical modeling indicate that if any rearranged complexes $\text{Y}^-(\text{RX})$ are formed in the ion source, they do not contribute to the metastable signal.

Metastable Dissociation and Collisional Activation. For the purpose of modeling the kinetic energy release data, it is important that the dissociations observed arise from metastable ions and not from collisional activation by residual background gases in the second field-free region (2FFR). To verify that the experiment is probing true metastable dissociation, the KERDs and branching ratios measured are compared to those obtained with helium added to the 2FFR collision cell to result in about 50% depletion in the main beam. The branching ratios and average kinetic energy releases for metastable and collisionally activated dissociation are collected in Table 1, and further details for the specific systems are given below.

A representative example of this comparison for the KERDs is shown in Figure 1 for the dissociation of $\text{Cl}^-(\text{CF}_3\text{CO}_2\text{CH}_3)$. (Plots of the experimental KERD data for metastable dissociation and CAD for the remaining three reactions are available as Supporting Information.) Two ionic products are observed, corresponding to cleavage of the electrostatic bond (eq 5a) and nucleophilic displacement (eq 5b). Equation 5b represents a half-reaction for the gas-phase $\text{S}_{\text{N}}2$ process, starting from the intermediate adduct species.



It can be seen that for both products, the KERD for collisionally activated dissociation (CAD) is significantly broader. This result is evidence that the dissociations leading to the narrower KERDs do not result from CAD with background gases, in which case

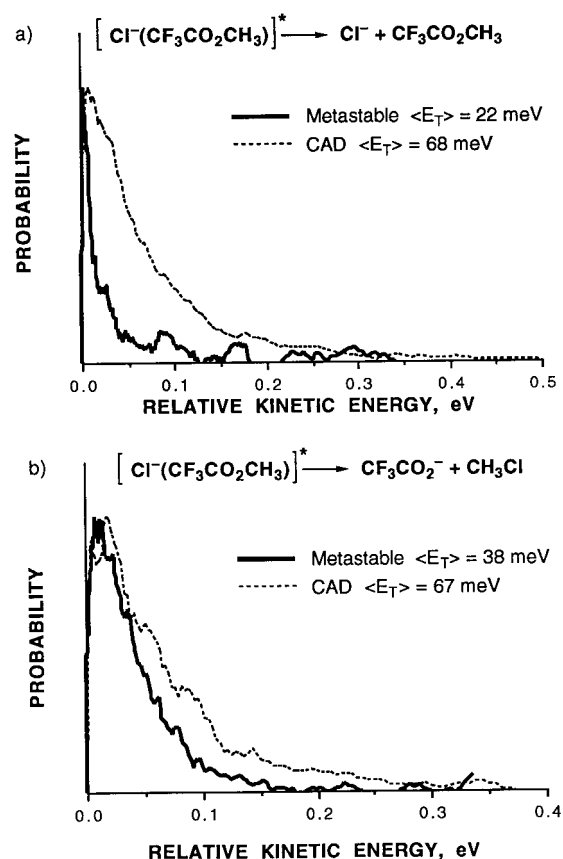
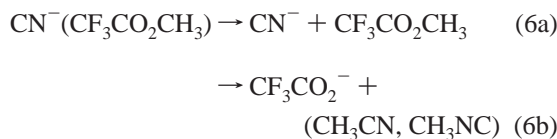


Figure 1. Experimental kinetic energy release distributions for metastable (heavy solid line) and collisionally activated (dashed line) dissociation of $\text{Cl}^-(\text{CF}_3\text{CO}_2\text{CH}_3)$: (a) back-dissociation to $\text{Cl}^- + \text{CF}_3\text{CO}_2\text{CH}_3$; (b) nucleophilic displacement to $\text{CF}_3\text{CO}_2^- + \text{CH}_3\text{Cl}$.

similar KERDs would be expected for both experiments. Additional evidence that the experiment probes true metastable dissociation can be found in the branching ratios observed for metastable dissociation vs CAD. Metastable dissociation of $\text{Cl}^-(\text{CF}_3\text{CO}_2\text{CH}_3)$ strongly favors channel 5b over 5a by a factor of 25. In contrast, CAD reverses the preference, and favors 5a over 5b by a factor of 4 (for target gas pressures that result in an increase of product ion signal of more than $10\times$). For the production of CF_3CO_2^- , the ion kinetic energy analysis for the metastable KERDs was repeated twelve times over the course of several days, and showed a highly reproducible average kinetic energy release of 38 ± 1 meV. The KERD for the Cl^- product from metastable dissociation was narrower, with an average release of 22 ± 6 meV.

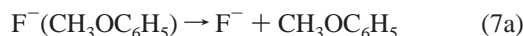
Significant differences in KERDs and branching ratios for metastable vs CA dissociation were observed for all four reactions, with one exception: the KERDs for the CF_3CO_2^- product from metastable and CA dissociation of $\text{CN}^-(\text{CF}_3\text{CO}_2\text{CH}_3)$ were similar. In this case, the relatively broad metastable KERD is probably a consequence of the large exothermicity of this reaction. The KERDs for the CN^- product in the two experiments were clearly different (with CAD giving a much broader KERD), and the branching ratios were very different for metastable dissociation vs CAD. Therefore we conclude that in all four systems, we are observing true metastable dissociation.

The metastable adduct from the reaction of CN^- with $\text{CF}_3\text{CO}_2\text{CH}_3$ dissociated to yield both CN^- and CF_3CO_2^- (eq 6), with a branching ratio of 50:1 in favor of channel 6b.



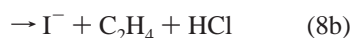
For CAD, however, when the target gas pressure was high enough to produce an increase in the product ion signal of about 30 \times , channel 6a was favored over channel 6b by 9:1. The vast majority of this increase corresponds to dissociation into channel 6a. This result demonstrates that CAD and metastable dissociation are distinct processes.

The dissociation of the metastable adduct of F^- with $\text{CH}_3\text{-OC}_6\text{H}_5$ yielded F^- and $\text{C}_6\text{H}_5\text{O}^-$ (eq 7), with a branching ratio of about 20:1 in favor of eq 7b.



Collisional activation results in channel 7a dominating by about 3:2, with an increase in total product ion signal of more than a factor of 40 for the target gas pressure used. In this system, the KERD for the F^- product is significantly broader than observed for eqs 5a and 6a, although it is still narrower than the corresponding KERD for collisional activation.

The adduct of Cl^- with $\text{CH}_3\text{CH}_2\text{I}$ was difficult to generate in abundance and the signals for the product ions from metastable dissociation were correspondingly weak. Only one fragment ion, I^- , was observed. We attribute this ion to the substitution reaction (eq 8a) rather than the elimination reaction (eq 8b), which is slightly endothermic ($\Delta H = 1.6$ kcal/mol). The latter channel would not be expected to compete effectively with the thermoneutral reversion to reactants or with the exothermic substitution reaction in metastable dissociation.



On the basis of the observed signal-to-noise ratio of the experiments, the branching ratio for Cl^- produced by metastable dissociation must be less than 2%. The experiment was repeated nine times and KERD analysis gave an average kinetic energy release of 46 ± 1 meV. When helium was admitted to the collision cell in the 2FFR for CAD experiments to give an increase of about 40 \times in the total product ion signal, both Cl^- and I^- were detected, in approximately 1:3 ratio favoring the I^- product. In the CAD experiments, eq 8b may also figure in the formation of I^- .

For these reactions, the ion source conditions (temperature and reactant pressure) under which the clusters could be generated were fairly limited. However, over the range available, no systematic variation in the average kinetic energy releases or the shapes of the KERDs could be observed.

Molecular Orbital Calculations. Although the overall thermochemistry for the bimolecular reactions studied is available from the literature, information about the relative energies, structures, and vibrational frequencies of the intermediate complexes and the transition states were lacking. Because such information is needed for the modeling of the KERDs by statistical phase space theory, ab initio molecular orbital calculations were performed. The possibility of isomeric species was also a concern for some of the ion-molecule complexes and transition states. For three of the reactions (eqs 1–3), initial

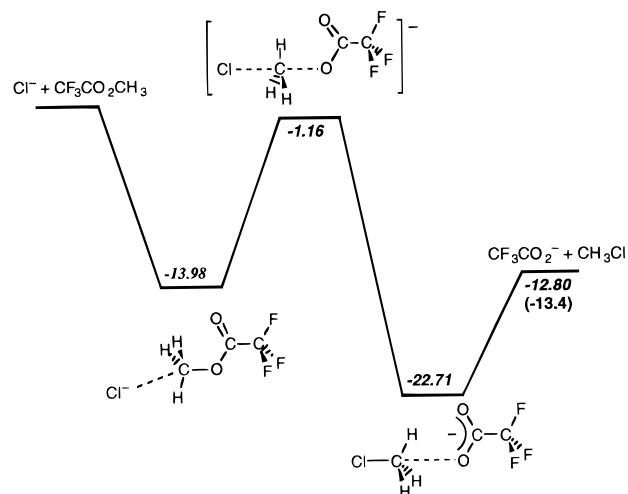


Figure 2. Calculated reaction coordinate for $\text{S}_{\text{N}}2$ reaction of Cl^- + $\text{CF}_3\text{CO}_2\text{CH}_3$. Relative energies shown are determined from MP2/6-31+g(d) single-point energies calculated at the HF/6-31+G(d) optimized geometries and corrected for zero-point vibrational energy. Literature thermochemistry is shown in parentheses and adjusted to 0 K.²⁹ Energies are given in kcal/mol.

searches for structures at local minima were made at the Hartree-Fock level by using the 3-21G basis set. Further optimization was performed for all degrees of freedom by using the 6-31+G(d) basis set. Frequency analysis was performed for these optimized geometries, and single point energies were then calculated at the MP2 level. At this level, good agreement was found with experiment for the overall 0 K enthalpy of the reactions of Cl^- and CN^- with $\text{CF}_3\text{CO}_2\text{CH}_3$. The agreement was less satisfactory for the reaction of F^- with $\text{CH}_3\text{OC}_6\text{H}_5$. For this reaction, the single-point MP2 calculations were performed with a larger basis set, 6-311+G(d,p), which yielded better agreement with the literature. For the reaction of Cl^- with $\text{CH}_3\text{CH}_2\text{I}$ (eq 4), full geometry optimizations were performed at the HF and MP2 levels by using the LANL1DZ basis set. Frequency analyses were performed at the HF level. For this reaction, the MP2 level gave better agreement with the overall experimental thermochemistry. Detailed structural information (in the form of \mathbf{z} -matrixes), total energies (hartrees), and zero-point vibrational energies (kcal/mol) are provided in The Supporting Information.

On the basis of the results of these calculations, schematic reaction coordinates were constructed for each of the reactions at 0 K. These are shown in Figures 2–4 for reactions 1–3. The relative energies are evaluated from the MP2 single point energies with zero-point vibrational energy included. For reaction 4, the relative energies are evaluated from the geometry-optimized MP2 values and corrected for the HF zero-point vibrational energies (Figure 5). Also shown are literature values for the overall reaction thermochemistry.^{29,34,35} These reaction coordinates were used for the statistical phase space theoretical modeling described in the next section.

For the reactions with $\text{CF}_3\text{CO}_2\text{CH}_3$, the optimized geometry for the reactant complex showed the nucleophile X bound at the methyl group approximately in line with the C–O bond, slightly closer to the hydrogen anti to the carboxyl group, as

(34) The heat of formation of $\text{CF}_3\text{CO}_2\text{CH}_3$ is estimated by using the additivity method of Benson (ref 35), by taking the difference between the known values of ΔH_f (ref 29) for $\text{CH}_3\text{CO}_2\text{CH}_3$ and CH_3COOH as an estimate for the incremental change in ΔH_f between $\text{CF}_3\text{CO}_2\text{CH}_3$ and $\text{CF}_3\text{-COOH}$. The estimated uncertainty is ± 3 kcal/mol.

(35) Benson, S. W. *Thermochemical Kinetics*; John Wiley & Sons: New York, 1968.

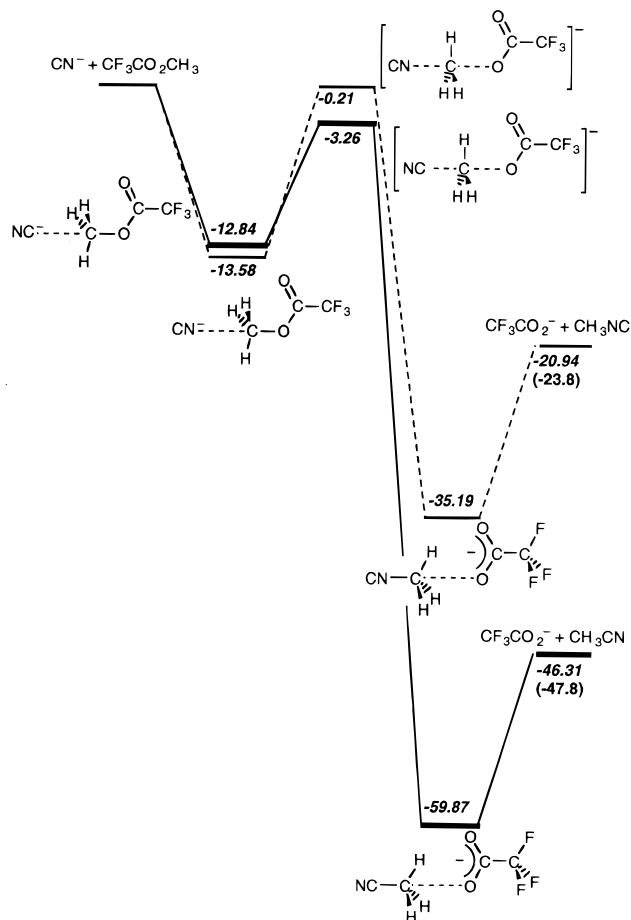


Figure 3. Calculated reaction coordinates for S_N2 reaction of CN^- + $CF_3CO_2CH_3$. Relative energies shown determined as in Figure 2. The solid line corresponds to nucleophilic attack by the carbon atom of CN^- , and the dashed line is for attack by the nitrogen atom. Literature thermochemistry is shown in parentheses and adjusted to 0 K.²⁹ Energies are given in kcal/mol.

shown in Figure 2. The X–C–O angle in this species is nearly linear: 165–170°. Two analogous isomeric structures were found for the reactant complex in the reaction of CN^- with $CF_3CO_2CH_3$, corresponding to attack by the carbon or nitrogen atom of CN^- . The latter structure is the more stable of the two by about 0.8 kcal/mol. No evidence was found for a tetrahedral intermediate resulting from nucleophilic addition at the carbonyl group.

In the reactant complex for the reaction of F^- with $CH_3OC_6H_5$, the F^- nucleophile was found to form a bridge between an ortho hydrogen of the phenyl ring and one of the hydrogens on the methyl group. This complex was bound by 23.5 kcal/mol, almost twice as strongly as the reactant complex species found for Cl^- and CN^- with $CF_3CO_2CH_3$. A second isomer was found in which the F^- was bound at the phenyl hydrogen para to the methoxy group. This structure was bound by about 16 kcal/mol at the highest level of theory used.

Coarse transition state searches were performed by starting with the optimized reactant complex structures and gradually decreasing the distance between the nucleophile and the carbon of the methyl group. That degree of freedom was fixed and all others were optimized. This process was repeated until the energy reached a maximum, at which point a transition state optimization was performed for all degrees of freedom. Frequency analysis confirmed for each optimized transition state that only one vibrational mode was imaginary, and this mode corresponded to the asymmetric stretch mode for the X–C–Y

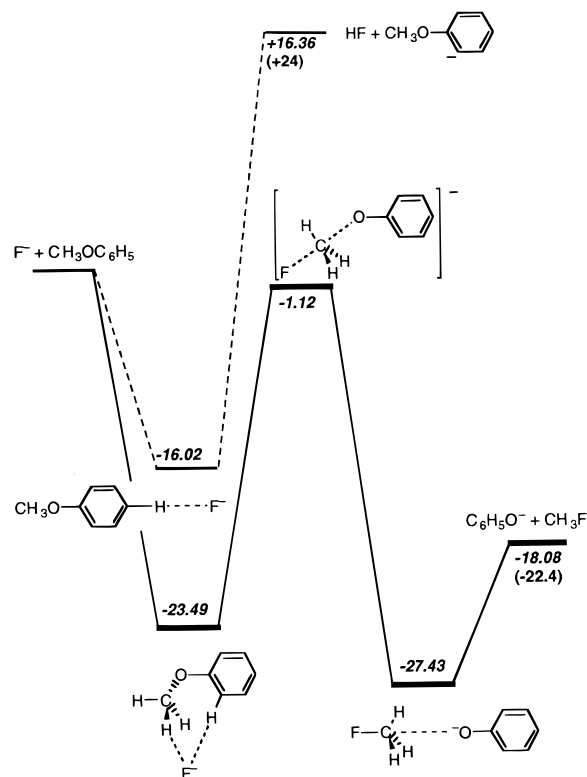


Figure 4. Calculated reaction coordinate for S_N2 reaction of F^- + $CH_3OC_6H_5$. Relative energies shown are determined from MP2/6-311+G(d,p) single-point energies calculated for the HF/6-31+G(d) optimized geometries and corrected for zero-point vibrational energy. The proton-transfer channel is shown as a dashed line and is endothermic overall. Literature thermochemistry is shown in parentheses and adjusted to 0 K.²⁹ Energies are given in kcal/mol.

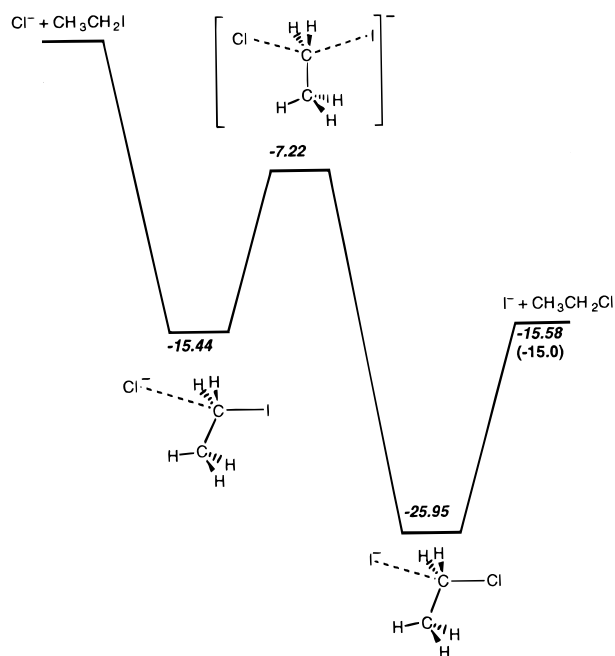


Figure 5. Calculated reaction coordinate for S_N2 reaction of Cl^- + CH_3CH_2I . Relative energies shown are determined from MP2/LANL1DZ optimized geometries and corrected for zero-point vibrational energy. Literature thermochemistry is shown in parentheses and adjusted to 0 K.²⁹ Energies are given in kcal/mol.

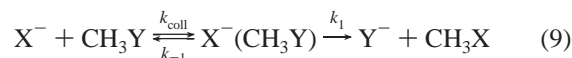
group, where X is the attacking atom of the nucleophile and Y the atom of the leaving group that is bound to the transferring methyl group. An interesting feature of the transition states

for the reactions involving $\text{CF}_3\text{CO}_2\text{CH}_3$ is that the methyl group rotates by 60° from its optimal position in the reactant complex, such that in the transition state a CH bond is eclipsed with the carboxyl group (see Figure 2). This rotation was observed to occur within the last 0.05 Å change in distance between the nucleophile and the methyl carbon, and the eclipsed conformation is retained in the product complexes. For reactions 1–3, the $\text{S}_{\text{N}}2$ transition states were found to be 1–3 kcal/mol below the energy of the separated reactants when zero-point energy was included. As can be seen in Figures 2–5, for all the transition states, the transferring methyl or ethyl group is nearly planar in the transition state.

It is interesting to compare the reactions of Cl^- and CN^- with $\text{CF}_3\text{CO}_2\text{CH}_3$. The cyanide reaction is significantly more exothermic, but the central barrier height (the transition state energy relative to the separated reactants) calculated for the carbon attack in the cyanide reaction is only slightly lower than that of chloride. The unimolecular substitution barrier, as measured by the energy difference between the reactant complex and the transition state, is about 9.6 kcal/mol. This is smaller than the chloride barrier of 12.8 kcal/mol (at the highest level of theory used), but is significantly greater than the substitution barrier for another $\text{S}_{\text{N}}2$ reaction of comparable exothermicity, $\text{F}^- + \text{CH}_3\text{Cl}$, which has been calculated to have a barrier of only 2.8 kcal/mol at 0 K, at the G2(+) level of theory.³⁶ According to Marcus theory as applied to gas-phase substitution reactions,^{4e} this would suggest a greater intrinsic substitution barrier for cyanide as compared to the halides. (The intrinsic barrier is the difference between the reactant complex and the transition state for the symmetric reaction $^*\text{X}^- + \text{CH}_3\text{X} \rightarrow \text{CH}_3^*\text{X} + \text{X}^-$). A greater intrinsic barrier would be consistent with the 30–40 kcal/mol greater energy of a C–C bond vs a C–Cl bond for both homolytic and heterolytic dissociation.^{29,37}

The calculations for the reaction of Cl^- with $\text{CH}_3\text{CH}_2\text{I}$ reproduce the literature value for overall reaction enthalpy quite well (Figure 5).²⁹ However, the central barrier height is somewhat lower than might be expected by comparison with the $\text{Cl}^- + \text{CH}_3\text{I}$ reaction, for which high-level calculations give the central barrier as -2.7 (MP2/PTZ+)³⁸ and -3.3 kcal/mol (G2+),³⁶ and a PST model of bimolecular kinetics gives -4.6 ± 0.4 kcal/mol.¹ The MP2 optimized geometries with the unaugmented LANL1DZ basis set give a central barrier of -7.2 kcal/mol (corrected for zero-point energy) for the $\text{Cl}^- + \text{CH}_3\text{CH}_2\text{I}$ reaction. This reaction is only slightly more exothermic than the $\text{Cl}^- + \text{CH}_3\text{I}$ $\text{S}_{\text{N}}2$ reaction, and the reaction efficiencies are about equal ($\sim 10\%$),^{5b} which would suggest comparable central barriers. As is shown below, the PST-ADO calculations give a central barrier of -3.5 ± 1.8 kcal/mol for reaction 4.

Theoretical Phase Space Calculations. Central barrier heights for the $\text{S}_{\text{N}}2$ reactions were evaluated by modeling the experimental reaction rate coefficients using statistical phase space theory with the average dipole approximation (PST-ADO). The details of the PST-ADO model are described in the Appendix, and only the results are presented here. The reaction kinetics were modeled with the assumption of steady-state conditions for a reactant complex that is formed at the collision rate (eq 9).



This allows the reaction probability, defined as $k_{\text{expt}}/k_{\text{coll}}$, to be related to the ratio of the rates of unimolecular dissociation of the reactant complex to the reactants vs $\text{S}_{\text{N}}2$ products. Thus,

$$\frac{k_{\text{expt}}}{k_{\text{coll}}} = \frac{k_1}{k_1 + k_{-1}} \quad (10)$$

where k_1 is the rate constant for passage through the $\text{S}_{\text{N}}2$ transition state. Reaction probabilities were calculated for a range of central barrier heights. These probabilities were then compared to the experimental efficiency, which was taken as the experimental rate coefficient divided by the collision rate constant.³⁹ These calculated reaction probabilities are most sensitive to the central barrier height and the values of the lowest frequency vibrational modes of the $\text{S}_{\text{N}}2$ transition state. The uncertainty in the calculated barrier heights was estimated by varying the lowest five frequencies of the transition state by $\pm 25\%$ and assuming error bars for the experimental rate coefficients of $\pm 30\%$. The resulting fitted barrier heights are collected in Table 2, along with the calculated transition state energies from the ab initio calculations. Also shown are the experimental reaction coefficients and the calculated collision rate constants that were used in the fitting.

The median calculated barrier heights from modeling the reaction kinetics were used in phase space modeling of the branching ratios for the metastable dissociations. If the metastable species is assumed to be the unstabilized ion–molecule collision complex (i.e., no stabilizing third-body collisions occur during the lifetime of the complex), the predicted branching ratio for metastable dissociation strongly favors dissociation to the reactants (channel a in eqs 5–8). In contrast, the calculated metastable branching ratios for fully thermally stabilized 270 K clusters strongly favor the $\text{S}_{\text{N}}2$ products. Taken together, these calculations suggest that the metastable species have undergone at least partial stabilization. The stabilization mechanism is probably low-energy collisions in the ion source, which should serve to relax the nascent internal energy distribution of the ion–molecule collision complex toward a thermal Boltzmann distribution. It therefore seems reasonable to assume that the true internal energy E and angular momentum J distributions of the metastable clusters will fall between these two extremes (nascent collision complex and thermally equilibrated), and that calculations assuming the two extreme cases may be used to “bracket” the experimental KERD results. It should be noted that these E and J distributions are further modified by the inclusion in the calculations of the probability of dissociation within the experimental time window. The effect of including this factor is to truncate the high-energy portion of the energy distributions. For simplicity, the E and J distribution functions for the two cases will hereafter be referred to as “CC” for the nascent collision complex and “Th” for a 270 K thermalized species, and the resulting KERDs will be labeled as such.

With use of these E and J distribution functions, statistical PST-ADO calculations were performed to predict kinetic energy release distributions for the metastable dissociations of the ion complexes. To test the sensitivity of the results to the values of the parameters used in the PST-ADO calculations, the central

(36) Glukhovtsev, M. N.; Pross, A.; Radom, L. *J. Am. Chem. Soc.* **1996**, *118*, 6273–6284.

(37) McMillen, D. F.; Golden, D. M. *Annu. Rev. Phys. Chem.* **1982**, *33*, 493–532.

(38) Hu, W.-P.; Truhlar, D. G. *J. Am. Chem. Soc.* **1995**, *117*, 10726–10734.

(39) Su, T.; Chesnavich, W. J. *J. Chem. Phys.* **1982**, *76*, 5183–5185. See also: Chesnavich, W. J.; Su, T.; Bowers, M. T. *J. Chem. Phys.* **1980**, *72*, 2641–2655. Chesnavich, W. J.; Su, T.; Bowers, M. T. *NATO ASI Series B—Physics*; Ausloos, P., Ed.; Plenum: New York 1979; Vol. 40, p 31ff.

Table 2. Comparison of Central Barrier Heights for the Following Reactions: $\text{Cl}^- + \text{CF}_3\text{CO}_2\text{CH}_3$, $\text{CN}^- + \text{CF}_3\text{CO}_2\text{CH}_3$, $\text{F}^- + \text{CH}_3\text{OC}_6\text{H}_5$, and $\text{Cl}^- + \text{CH}_3\text{CH}_2\text{I}$

reactants	$k_{\text{coll}},^a \text{ cm}^3/\text{s}$	$k_{\text{expt}}, \text{ cm}^3/\text{s}$	$\Delta E^\ddagger(\text{kinetics}),^b \text{ kcal/mol}$	$\Delta E^\ddagger(\text{ab initio}),^c \text{ kcal/mol}$	$\Delta E^\ddagger(\text{KERD}),^d \text{ kcal/mol}$
$\text{Cl}^- + \text{CF}_3\text{CO}_2\text{CH}_3$	2.79×10^{-9}	$1.29 \times 10^{-10} \text{ }^e$ $0.45 \times 10^{-10} \text{ }^f$	-1.4 ± 1.6	-1.16	-2.0 [0.0 to -5.3]
$\text{CN}^- + \text{CF}_3\text{CO}_2\text{CH}_3$	3.09×10^{-9}	$1.05 \times 10^{-10} \text{ }^e$ $0.3 \times 10^{-10} \text{ }^f$	-2.3 ± 1.6	-3.26	-3.7 [-1.8 to -4.6]
$\text{F}^- + \text{CH}_3\text{OC}_6\text{H}_5$	2.63×10^{-9}	$0.8 \times 10^{-10} \text{ }^f$ $(5.7 \times 10^{-10} \text{ }^e)^g$	-3.3 ± 1.6	-1.09	-3.7 [-3.1 to -4.6]
$\text{Cl}^- + \text{CH}_3\text{CH}_2\text{I}$	2.11×10^{-9}	$2.07 \times 10^{-10} \text{ }^e$	-3.5 ± 1.8	-7.22	-4.6 [-1.7 to -7.0]

^a Collision rate constant calculated by using the variational transition state method, ref 39. ^b Central barrier heights determined from fitting experimental kinetics by using statistical phase space theory (PST-ADO). ^c Central barrier heights from ab initio calculations. ^d Central barrier height from fitting KERD. In brackets are shown the ranges of barrier heights considered for fitting. ^e Grabowski and Owusu, flowing afterglow results, private communication. ^f Reference 4c. ^g Not used in modeling; third-body enhancement of rate suspected based on observation of clustering of reactants.

barrier heights were varied over the complete range given by the ab initio calculations plus the PST-ADO modeling of the bimolecular reaction kinetics. In addition, the binding energies for the complexes were varied from the ab initio values by $\pm 25\%$ and the lowest five vibrational frequencies of the transition states were varied by $\pm 25\%$. Although the experimental KERDs for the simple back-dissociation could be bracketed by the calculated KERDs for the CC and Th distribution functions, the experimental KERDs for the $\text{S}_{\text{N}}2$ products were always considerably narrower than both the calculated KERDs, indicating that products were translationally cold and internally hot relative to the predictions of statistical theory. The effect of internal excitation in the $\text{S}_{\text{N}}2$ products was modeled by decreasing the reaction exothermicity and calculating the effective KERD, and the best fits are presented below. For clarity of presentation, the experimental and calculated KERDs are scaled to the same maximum.

In Figure 6a are shown calculated and experimental KERDs for the dissociation of $\text{Cl}^-(\text{CF}_3\text{CO}_2\text{CH}_3)$ to give Cl^- and $\text{CF}_3\text{CO}_2\text{CH}_3$. This calculation was found to be most sensitive to the value of complex binding energy and the central barrier height. Increasing the binding energy or raising the central barrier had the effect of broadening the calculated KERD, due to an increased complex lifetime, such that higher energy complexes move into the metastable time window. The results shown were obtained for a binding energy of 14.0 kcal/mol (from the ab initio calculations) and a central barrier height of -2.0 kcal/mol, a value that was found by trial and error to give the best fits for the $\text{S}_{\text{N}}2$ dissociation (see below). The CC and Th KERDs bracket the experimental result at relative kinetic energies below about 0.04 eV. The high-energy "tail" in the experimental distribution at relative kinetic energies greater than 0.04 eV is probably due to the occurrence of a small amount of CAD, which strongly enhances this dissociation channel (Table 1). As can be seen in Figure 1, the KERD for the Cl^- product from CAD extends well beyond 0.15 eV relative energy.

The same parameters were used to calculate the KERD for the CF_3CO_2^- product, and the CC (solid line) and Th (dashed line) KERDs are shown in Figure 6b along with the experimental result. Both calculated curves are clearly broader than the experimental KERD. For the CC distribution, decreasing the central barrier height over the range shown in Table 2 results in broadening of the calculated KERD and a shift of the energy of maximum probability to higher energies. The Th KERD is wider than the experimental data and does not reproduce the energy dependence well, showing a maximum probability at 0.00 eV and higher probabilities for large kinetic energies than in the experimental distribution. Lowering the barrier height narrowed the calculated KERD, but did not result in any

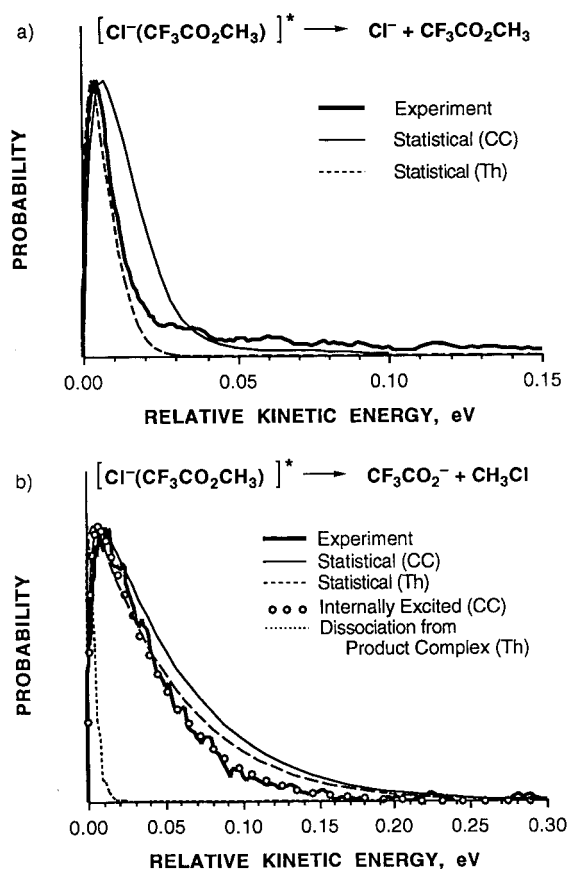


Figure 6. Experimental and theoretical KERDs for metastable dissociation of $\text{Cl}^-(\text{CF}_3\text{CO}_2\text{CH}_3)$. (a) KERDs for products from back-dissociation to $\text{Cl}^- + \text{CF}_3\text{CO}_2\text{CH}_3$: experimental data (heavy solid line); calculated with CC distribution (light solid line); calculated with Th distribution (dashed line). (b) KERDs for displacement products $\text{CF}_3\text{CO}_2^- + \text{CH}_3\text{Cl}$: experimental data (heavy solid line); statistical dissociation calculated with CC distribution (light solid line); statistical dissociation calculated with Th distribution (dashed line); CC with internal excitation $E_{\text{fix}} = 0.25$ eV (open circles); dissociation from a thermalized product complex (dotted line).

satisfactory fits. (An example of the variation of the calculated KERDs with barrier height is included in the Supporting Information.) The open circles in Figure 6 show the calculated KERD that is obtained with the CC distribution by decreasing the exothermicity of the reaction from -13.4 kcal/mol to -7.6 kcal/mol, a change of $+5.8$ kcal/mol. The agreement with experiment is excellent. For the Th distributions, the fit of the calculated KERDs to the experimental data was not improved greatly by changing the reaction exothermicity. Although the calculated KERDs narrowed somewhat as the exothermicity was

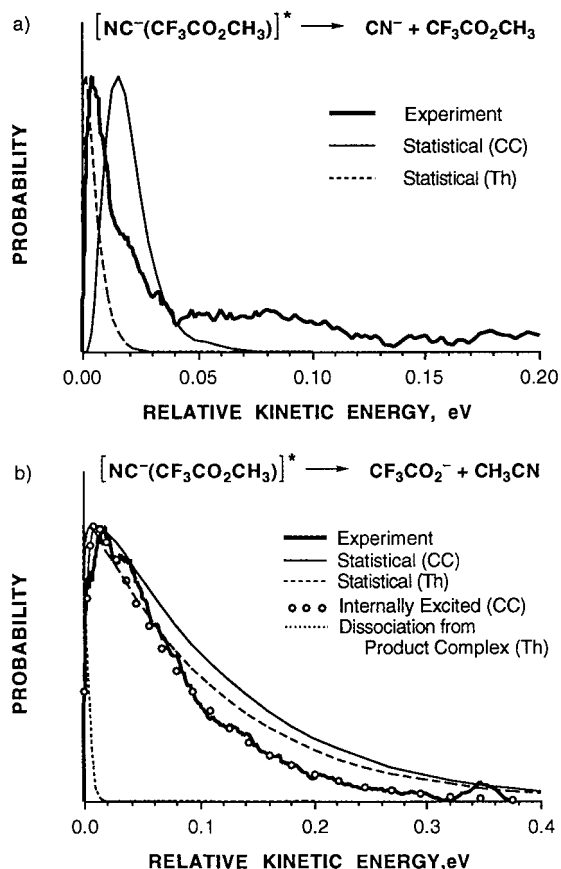


Figure 7. Experimental and theoretical KERDs for metastable dissociation of $\text{CN}^-(\text{CF}_3\text{CO}_2\text{CH}_3)$. (a) KERDs for products from back-dissociation to $\text{CN}^- + \text{CF}_3\text{CO}_2\text{CH}_3$: experimental data (heavy solid line); calculated with CC distribution (light solid line); calculated with Th distribution (dashed line). (b) KERDs for displacement products $\text{CF}_3\text{CO}_2^- + \text{CH}_3\text{CN}$: experimental data (heavy solid line); statistical CC (light solid line); statistical Th (dashed line); CC with $E_{\text{fix}} = 0.9$ eV (open circles); dissociation from a thermalized product complex (dotted line).

reduced, they all peaked at 0.0 eV and the probability fell off less steeply with energy than the experimental curve does. For this reaction, the change required in the reaction thermochemistry is about the same as the estimated uncertainty of ± 5 kcal/mol in the reaction thermochemistry.³⁴

Because these ion complexes are formed under conditions where partial collisional stabilization may occur, it is possible that the experimental KERD results from dissociation of a species trapped in the product complex well and partially thermalized. To determine whether this could yield the narrow experimental KERD, the KERD expected for such a situation was calculated. The very narrow curve shown as a dotted line in Figure 6b corresponds to the dissociation of a 300 K product complex $\text{CF}_3\text{CO}_2^-(\text{CH}_3\text{Cl})$. This result is only very weakly sensitive to the assumed temperature of the internal energy distribution and depends most strongly on the binding energy of the complex. The distribution shown was calculated for a product complex binding energy of 14 kcal/mol, and is clearly much narrower than the experimental result. The binding energy parameter had to be increased to more than 35 kcal/mol to reproduce the width of the experimental KERD. However, this is unreasonably large for an ion-dipole complex.²⁹

The experimental and calculated KERDs for dissociation of $\text{CN}^-(\text{CF}_3\text{CO}_2\text{CH}_3)$ to give CN^- and $\text{CF}_3\text{CO}_2\text{CH}_3$ are shown in Figure 7a. The KERDs shown were calculated for a central barrier height of -3.7 kcal/mol (relative to reactants) and a

complex binding energy of 12.9 kcal/mol. These values compare favorably with both the results of the ab initio calculations (Figure 3), and the central barrier height falls within the range calculated with PST-ADO theory for the bimolecular reaction (Table 2). In this case, the effect of the internal energy distribution is more noticeable, and the CC and Th curves bracket the experimental result, as might be expected if the experiment probes a partially stabilized species. The long tail of the experimental curve is most likely due to a small amount of collisional activation. As mentioned previously, CAD not only results in a much broader KERD for the simple back-dissociation process but also strongly favors that channel.

Calculation of the $\text{S}_{\text{N}}2$ KERD for this reaction is complicated by the possible competition between carbon and nitrogen attack. At the highest level of theory employed, the N-attack transition state is about 3.3 kcal/mol higher in energy than the C-attack transition state and 0.7 kcal/mol higher than the separated reactants. For these central barrier heights, the predicted branching ratio from PST-ADO is essentially 100% carbon attack, both for the bimolecular reaction and for the metastable reaction. On the basis of this branching ratio, we conclude that the nitrogen attack channel can be neglected for the purposes of calculating the KERD. The KERDs shown in Figure 7b were calculated for statistical dissociation with the CC (solid line) and Th (dashed line) distribution. Both curves are significantly broader than the experimental result. The KERD plotted with open circles is the result obtained with the CC energy distribution and assuming that the exothermicity of the reaction is only -26.7 kcal/mol instead of the -47.6 kcal/mol given by literature thermochemistry (corrected to 0 K). The fourth set of data (dotted line) corresponds to metastable dissociation of a thermalized (300 K) product complex $\text{CF}_3\text{CO}_2^-(\text{CH}_3\text{CN})$, and is clearly much narrower than the experimental result. This KERD was calculated by using a complex binding energy of 13.6 kcal/mol relative to separated products, as given by the ab initio calculations.

In Figure 8, the results for the metastable dissociation of the $\text{F}^-(\text{CH}_3\text{OC}_6\text{H}_5)$ complex are shown. The experimental KERD for back-dissociation to F^- and $\text{CH}_3\text{OC}_6\text{H}_5$ can be reproduced (except for the high-energy tail) by using the CC energy distribution with a complex binding energy of 23.5 kcal/mol, as given by the ab initio calculations, and a central barrier height of -3.7 kcal/mol (Figure 8a), in good agreement with the value determined by fitting the bimolecular kinetics (Table 2). The calculated KERD for the 270 K Th distribution, however, is considerably narrower than the experimental result, which suggests that a large fraction of the metastable complexes has not undergone significant stabilization. The same input parameters were used for the $\text{S}_{\text{N}}2$ dissociation with the CC and Th distributions, and yielded the curves shown in Figure 8b. As with the other systems, these two curves are broader than the experimental results. The curve plotted with open circles was obtained with the CC distribution and an effective exothermicity of -9.7 kcal/mol, rather than the -22.4 kcal/mol from the literature (corrected to 0 K). The KERD calculated for dissociation of a thermally equilibrated 270 K product complex $\text{C}_6\text{H}_5\text{O}^-(\text{CH}_3\text{F})$ is much narrower than the experimental KERD.

In Figure 9 are shown KERDs calculated for the dissociation of $\text{Cl}^-(\text{CH}_3\text{CH}_2\text{I})$ with the CC distribution (solid line) and the Th distribution (dashed line) for a central barrier height of -4.6 kcal/mol relative to the separated reactants. Both calculated curves are clearly broader than the experimental KERD, but the CC distribution more nearly reproduces the shape. The open circles in Figure 9 show the calculated KERD that is obtained

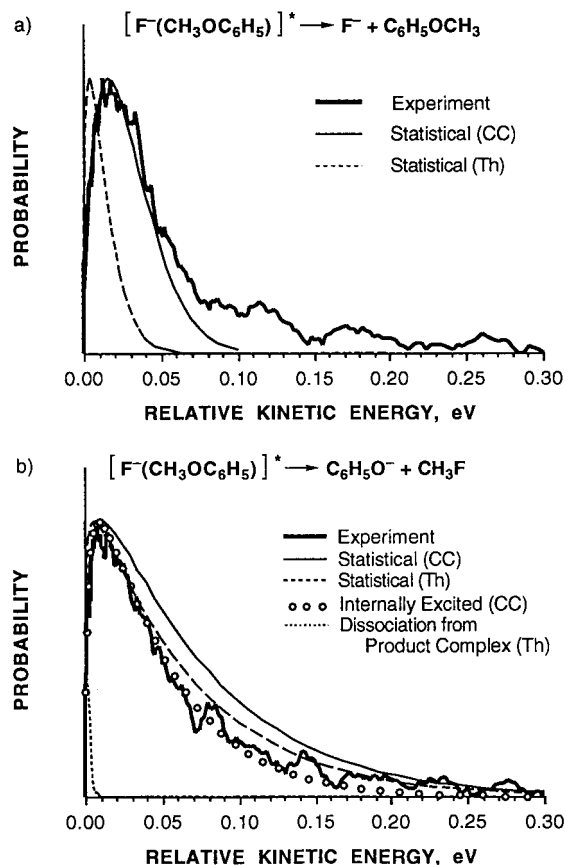


Figure 8. Experimental and theoretical KERDs for metastable dissociation of $F^-(CH_3OC_6H_5)^*$. (a) KERDs for products from back-dissociation to $F^- + CH_3OC_6H_5$: experimental data (heavy solid line); calculated with CC distribution (light solid line); calculated with Th distribution (dashed line). (b) KERDs for displacement products $C_6H_5O^- + CH_3F$: experimental data (heavy solid line); statistical CC (light solid line); statistical Th (dashed line); CC with $E_{fix} = 0.55$ eV (open circles); dissociation from a thermalized product complex (dotted line).

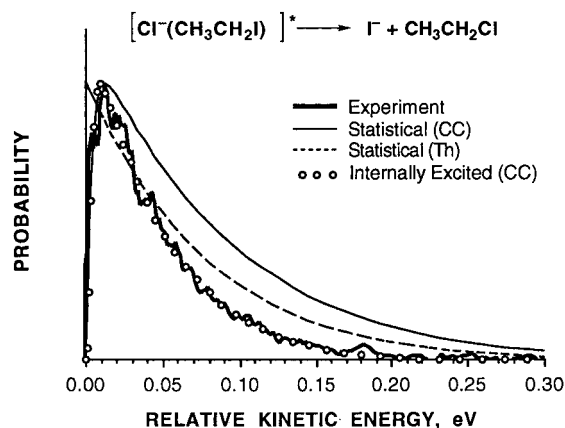


Figure 9. Experimental and theoretical KERDs for metastable dissociation of $Cl^-(CH_3CH_2I)^*$ to give the displacement products $I^- + CH_3CH_2Cl$: experimental data (heavy solid line); statistical CC (light solid line); statistical Th (dashed line); CC with $E_{fix} = 0.45$ eV (open circles).

with the CC distribution by decreasing the exothermicity of the reaction from the literature value of -15.0 kcal/mol to -4.6 kcal/mol. The agreement with experiment is quite good. However, this exothermicity is well outside the combined uncertainty of the reaction thermochemistry. Under the conditions of our experiment, the PST-ADO calculations predict that product complexes $I^-(CH_3CH_2Cl)$ with internal energy above the dissociation threshold dissociate before reaching the second

field-free region. Therefore, no curve is shown for the dissociation of a stabilized product complex.

Discussion

As mentioned in the Introduction, our goal is to study the unimolecular dissociation of the chemically activated intermediate complexes of a bimolecular nucleophilic substitution reaction. Of particular interest is the dissociation that corresponds to passage through the S_N2 transition state, and whether this is a statistical process. In our earlier study of metastable dissociation of halide–methylhalide complexes,¹ statistical phase space modeling of the experimental results led to the conclusion that the neutral species were vibrationally excited well beyond what would be predicted by statistical partitioning of the available reaction energy. The present study considers four relatively disparate examples of carbon-centered nucleophilic substitution, with widely different reaction exothermicities, polyatomic nucleophiles, and leaving groups, many more internal degrees of freedom than in the methylhalide reactions, and, in one case (eq 3), a hydrogen-bonded reactant complex, which is significantly more strongly bound and therefore longer lived than any of the other complexes (Figure 4). Yet the results of the theoretical modeling again indicate that the products of nucleophilic substitution are internally excited.

In Table 3, the amounts of unavailable (fixed) energy, E_{fix} , that had to be deducted from the reaction exothermicities to produce the fits shown in Figures 6–9 are listed and compared to various reaction parameters. There is a good correlation of E_{fix} with overall reaction exothermicity ΔH_{rxn} and no apparent correlation with the number of vibrational degrees of freedom N_{vib} of the intermediate complexes. In all cases, the value of E_{fix} is a significant fraction ($>40\%$) of the reaction exothermicity, and is moreover large enough to accommodate several vibrational quanta in modes such as the umbrella motion of the CH_3 group and the stretch of the newly formed C–X bond (X being the nucleophile). One conclusion that may be drawn from this observation is that there is relatively little randomization of the energy stored in these modes after passage through the transition state region.

In the $X^-(RY)$ complexes, several low-frequency vibrational modes are associated with stretching and bending about the electrostatic $X^- - RY$ bond. For the case of $Cl^-(CH_3Br)$ or $Cl^-(CH_3Cl)$, these modes are significantly lower in frequency than the modes associated primarily with the CH_3Br or CH_3Cl moiety. For the purpose of this discussion, these two sets of vibrational modes will be called “intermoiety” and “intramoiety”, respectively. Hase and co-workers have suggested that poor coupling between the low-frequency intermoiety and higher frequency intramoiety vibrational modes of the intermediate complexes in halide–methylhalide reactions causes incomplete randomization of energy.²² The noncorrelation of E_{fix} with N_{vib} would support this conclusion; the number of intramoiety modes in the intermediate complex has no discernible impact on the internal excitation of the products. However, the energy gap between the inter- and intramoiety modes for these complexes is considerably smaller than in the case of $Cl^-(CH_3Cl)$ and $Cl^-(CH_3Br)$. The fifth column of Table 3 shows the vibrational frequencies corresponding to the intermoiety modes and, in parentheses, the lowest two intramoiety modes for the product complexes. For all four reactions, the energy gap between the inter- and intramoiety modes is less than 200 cm^{-1} , but for the first two reactions listed, the lowest frequency vibrational mode (6 and 8 cm^{-1}) corresponds to an intramoiety mode, rotation of the CF_3 group.

Table 3. Internal Excitation in Substitution Products and Various Experimental and Fitted Parameters

reactants	E_{fix} , ^a kcal/mol	ΔH_{rxn} , ^b kcal/mol	N_{vib} ^c	ν , cm ⁻¹ intermoiety (intramoiety) ^d	τ , ^e s
Cl ⁻ + CF ₃ CO ₂ CH ₃	5.8 (43%)	-13.4	30	14, 29, 52, 60, 74, 90 (8, 247)	2.1×10^{-12}
CN ⁻ + CF ₃ CO ₂ CH ₃	20.8 (44%)	-47.6	33	14, 28, 31, 60, 80, 106 (6, 248)	1.5×10^{-12}
F ⁻ + CH ₃ OC ₆ H ₅	12.7 (57%)	-22.4	45	4, 10, 11, 76, 81, 82 (194, 419)	1.8×10^{-10}
Cl ⁻ + CH ₃ CH ₂ I	10.4 (69%)	-15.0	21	42, 47, 71 (249, 302)	7.5×10^{-12}

^a Energy that is unavailable for randomization, as determined from fitting experimental KERDs by using statistical phase space theory (PST-ADO). The values in parentheses show the unavailable energy as a percent of reaction exothermicity. ^b Overall S_N2 reaction enthalpy, 0 K. ^c Number of vibrational degrees of freedom for intermediate ion–molecule complexes. ^d Intermoiety and (lowest two intramoiety) vibrational frequencies for product complexes. See text of Discussion for explanation of “intermoiety” and “intramoiety”. ^e PST-ADO lifetime of product complexes after passage over TS.

The last column of Table 3 shows lifetimes calculated with PST-ADO for the product complexes formed by passage over the substitution barrier for reactions 1–4. These lifetimes correspond to statistical dissociation of metastable complexes with the CC distribution, and therefore reflect the lifetimes for the population observed in the MIKES experiment. It might be expected that the shortest-lived product complexes would show the greatest deviations from statistical energy partitioning, but such a correlation is not apparent. However, in all cases, the predicted lifetime for statistical dissociation is quite short. In the S_N2 reactions described here, the transition state structures are significantly distorted from the product geometry. The distorted structure of the S_N2 transition state and the very short lifetime of the product complex result in significant amounts of energy being stored in vibrational modes of the products, with the result that the experimental kinetic energy distributions are narrower than predicted by theory.

We have shown that statistical dissociation of the reactant complexes formed in reactions 1–4 cannot lead to the observed KERDs for the S_N2 products unless the products are assumed to be internally excited. As outlined in the Results section, we have considered the possibility that the narrow KERDs result from dissociation of complexes trapped in the product well by low-energy collisions in the ion source, and have found that the statistical dissociation of such complexes would yield KERDs very much narrower than the observed results (Figures 6–8), or would yield no metastable signal (Figure 9), thus ruling out contributions from trapped product complexes. Recently, Viggiano and Hase and co-workers proposed that tunneling through the S_N2 barrier is implicated in the unimolecular dissociation to Br⁻ and CH₃Cl of Cl⁻(CH₃Br) formed by the endothermic solvent-switching reaction of CH₃Br with Cl⁻(H₂O).⁴⁰ Although our results indicate that some collisional stabilization occurs in the ion source, we are confident that tunneling does not contribute significantly to the KERDs we observe for these metastable dissociations. Phase space calculations show that even fully thermalized complexes have adequate internal energy for classical passage over the barrier, with probabilities on the order of 10⁻³ to 10⁻⁶ that this dissociation occurs on the metastable time scale (~10⁻⁵ s), consistent with experimental observation of a metastable dissociation signal.

An important feature of the PST-ADO calculations is that a self-consistent set of input parameters could be identified that reproduced the KERDs for both the back-dissociation and nucleophilic substitution (with the caveat that the reaction exothermicity is a variable parameter), and that these parameters were moreover in acceptable agreement with those given by

modeling the bimolecular kinetics or by the ab initio calculations. As is shown in Table 2, the optimized S_N2 barrier heights from PST-ADO modeling of the metastable dissociation KERDs are slightly lower than those derived from modeling the bimolecular reaction rate coefficients, but in all cases are well within the uncertainties. The agreement with ab initio calculations is not as good, but the level of calculation used here is only moderate and we consider the PST-ADO results to be more reliable. The KERD analysis indicates clearly that partitioning of energy in these metastable dissociations is not statistical. The time scale of the metastable experiment guarantees that the vibrational energy in these complexes is randomized, so the nonstatistical dissociation dynamics must be associated with passage through the S_N2 transition state. If the bimolecular reaction kinetics are correctly described by the steady-state model shown in eqs 9 and 10, then the good agreement between the energies of the S_N2 barriers derived for these two experiments (bimolecular reaction vs metastable unimolecular dissociation) suggests that the vibrational energy in intermediate complexes in the bimolecular reactions is also largely randomized.

Conclusions

The kinetic energy release distributions (KERDs) for metastable dissociation of four ion–molecule complexes have been measured by mass-analyzed ion kinetic energy spectroscopy and modeled with a combination of ab initio molecular orbital calculations and statistical phase space theory with the average dipole orientation approximation. The complexes correspond to intermediates in bimolecular S_N2 reactions. In each case, the experimental KERD is significantly narrower than would be predicted by phase space theory. A model for metastable dissociation that includes an adjustable parameter for internal excitation in the products is able to account for the nonstatistical experimental KERDs. There is a strong correlation between the magnitude of the internal excitation (E_{fix}) and the overall exothermicity of the reaction, and an inverse correlation with the lifetime of the product complex that is formed after passage over the S_N2 barrier.

Acknowledgment. This work was supported in part by the National Science Foundation through grants CHE-9502038 (S.T.G.) and CHE-9421176 (M.T.B.). S.T.G. also gratefully acknowledges support from the American Chemical Society Petroleum Research Fund in the form of a Type G grant (27088-G6) and a research award from the American Society for Mass Spectrometry. We are very grateful to Prof. J. J. Grabowski and Mr. Daniel Owusu for measuring the bimolecular rate coefficients for these reactions and communicating the results,

(40) Seeley, J. V.; Morris, R. A.; Viggiano, A. A.; Wang, H.; Hase, W. *J. Am. Chem. Soc.* **1997**, *119*, 577–584.

and we thank Dr. A. Viggiano and Prof. W. Hase for useful discussion. S.T.G. is grateful to Dr. L. M. Bass for helpful discussion in modifying the phase space theory computer code to incorporate the ADO potential.

Appendix

The PST-ADO Method. For these phase space calculations, we used the formalism developed by Bass and Bowers for the average dipole orientation (ADO) potential for long-range ion–dipole interactions.⁴¹ In this formalism, the long-range potential is given by eq 11 for a point charge interacting with a point dipole,

$$V_{\text{eff}}(L,r,\theta) = \frac{L^2\hbar^2}{2r^2} - \frac{q^2\alpha}{2r^4} - \frac{q\mu_D}{r^2} \cos \theta \quad (11)$$

where L is the orbital angular momentum quantum number, r is the separation between the charge and dipole, q is the charge on the ion, α is the polarizability of the dipole, μ_D is the dipole moment, and θ is the angle between the charge–dipole line of centers and the dipole orientation. For this effective potential, there is a maximum referred to as the centrifugal barrier located at r_k , defined by:

$$\left(\frac{dV_{\text{eff}}(L,r)}{dr}\right)_{r_k} = 0 \quad (12)$$

As was shown by Bass and Bowers, the minimum translational energy E_t^\ddagger required to surmount the centrifugal barrier for this potential can be expressed as:

$$E_t^\ddagger(r_k) = \frac{q^2\alpha}{2r_k^4} - \frac{q\mu_D}{2r_k} \left(\frac{d \cos \theta(r)}{dr}\right) \quad (13)$$

The maximum orbital angular momentum quantum number L^* for which passage over the centrifugal barrier is possible can be expressed as:

$$L^*(r_k) = \left[2r_k^2 \mu E_t^\ddagger(r_k) + \frac{q^2\alpha\mu}{r_k^2} + D^2\hbar^2 \cos \theta(r_k) \right]^{1/2} \quad (14)$$

where

$$D^2 = \frac{2\mu q\mu_D}{\hbar^2} \quad (15)$$

An average value $\langle \cos \theta \rangle$ for the dipole orientation term and its derivative are calculated numerically for the appropriate temperature of the dipole and as a function of the separation between the dipole and charge, r .⁴² By evaluating eqs 13 and 14 for a series of r_k values, a set of $\{E_t^\ddagger, L^*\}$ is obtained for the orbiting transition states at separation r . These values are then used to determine the limits of integration for the calculation of available phase space.

Parameters. Depending on the specifics of each calculation, several species enter into the model. In general, the important species include the orbiting transition states for association of the separated reactants or products, the reactant and product complexes (ion–dipole complexes), and the S_N2 transition state. The relative heats of formation at 0 K are taken from the

literature when available or from the ab initio relative energies, corrected for zero-point vibrational energies. The S_N2 transition state energy is evaluated by three different methods: ab initio calculations, PST-ADO modeling of the bimolecular kinetics, and PST-ADO fitting of the experimental KERDs. For the product orbiting transition states, the relative heats of formation comes from the literature. The relative heats of formation for the reactant and product complexes were taken from the ab initio calculations.

Experimental vibrational frequencies are used where available.⁴³ For other species, the vibrational frequencies are taken from the ab initio calculations at HF/6-31+G(d) and scaled by 0.89. The rotational constants used in the phase space calculations are the geometric mean of the rotational constants yielded by the ab initio calculations. Molecular polarizabilities were taken from the literature⁴⁴ or estimated by using the method of Miller and Savchik.⁴⁵

Tables of the parameters used in these calculations are provided as Supporting Information.

Internal Energy and Total Angular Momentum Distributions. For an ensemble of nascent ion–molecule complexes formed by thermal energy capture collisions at temperature T , the probability distribution of internal energy E and total angular momentum J may be expressed by eq 16:

$$P_{\text{CC}}(E,J;T) dE dJ = \frac{\int_0^E dE_t \exp(-E_t/k_B T) \int_0^{E-E_t} dE_v P(E_v, E_t) dJ_2 J F_1^{\text{orb}}(E, J)}{\int_0^\infty dE_t \exp(-E_t/k_B T) \int_0^\infty dE_v P(E_v, E_t) \int_0^{J_{\text{max}}} dJ_2 J F_1^{\text{orb}}(E, J)} \quad (16)$$

where E is zero for the separated reactants at 0 K, E_t is the relative translational energy of the reactants, E_r and E_v are the reactant rotational and vibrational energy, respectively, and $F_1^{\text{orb}}(E, J)$ is the flux through the orbiting transition state for total energy E and angular momentum J . In this expression, $P(E_v, E_r)$ is the probability for the reactants having vibrational energy E_v and rotational energy E_r :

$$P(E_v, E_r) = 2\rho(E_v) [(E - E_t - E_v)/B_r] \exp[-(E - E_t - E_v)/k_B T] \quad (17)$$

where $\rho(E_v)$ is the density of vibrational states for reactant vibrational energy E_v and B_r is the reduced rotational constant of the reactants. The function in eq 16 is referred to in the text as the CC distribution, for “collision complex”.

If the complex formed by association in the ion–molecule complex is brought to thermal equilibrium by low-energy collisions, the probability distribution of internal energy E and total angular momentum J may be expressed by:

$$P_{\text{Th}}(E,J;T) dE dJ = \frac{\int_0^E dE_v P(E_v, E_t) dJ_2 J \exp(-B_{\text{RC}} J^2/k_B T)}{\int_0^\infty dE_v P(E_v, E_t) \int_0^{J_{\text{max}}} dJ_2 J \exp(-B_{\text{RC}} J^2/k_B T)} \quad (18)$$

where the zero of energy is now taken as the zero point of the

(43) Shimanouchi, T. *Tables of Molecular Vibrational Frequencies*; National Bureau of Standards: Washington, DC, 1972; Consolidated Vol. 1.

(44) Radzig, A. A.; Smirnov, B. M. *Reference Data on Atoms, Molecules, and Ions*; Springer-Verlag: Berlin, 1985.

(45) Miller, K. J.; Savchik, J. A. *J. Am. Chem. Soc.* **1979**, *101*, 7206–7213.

(41) Bass, L. M.; Bowers, M. T. *J. Chem. Phys.* **1987**, *86*, 2611–2616.

(42) Bass, L. M.; Su, T.; Chesnavich, W. J.; Bowers, M. T. *Chem. Phys. Lett.* **1975**, *34*, 119–122.

reactant complex and B_{RC} is the rotational constant of the pre-reaction complex. The functional form of $P(E_v, E_r)$ is given by eq 19 for $E_v + E_r = E$.

$$P(E_v, E_r) = \rho_v^c(E_v) 2 \left(\frac{E - E_v}{B_{RC}} \right) \exp[-(E - E_v)/k_B T] \quad (19)$$

In this equation, $\rho_v^c(E_v)$ is the density of vibrational states for the ion cluster at vibrational energy E_v . The function given in eq 18 is referred to in the text as the Th distribution for a thermalized ion cluster.

Each of these energy distributions is further modified by a factor that accounts for the probability of dissociation within the experimental time window of about 10–20 μ s. This factor is calculated by using eq 20,

$$P_{\text{diss}}(E, J) = \exp(-k(E, J)t_1) - \exp(-k(E, J)t_2) \quad (20)$$

where $k(E, J)$ is the calculated rate of dissociation of the metastable complex of internal energy E and total angular momentum J , and t_1 and t_2 are the times of entry to and exit from the second field-free region of the mass spectrometer.

Calculation of ΔH^\ddagger . For the calculation of ΔH^\ddagger , it is assumed that the pre-reaction complex is formed in the bimolecular reactions at the collision rate k_{coll} , as given by the variational method of Su and Chesnavich.³⁹ It is also assumed that the experimental rate coefficients correspond to the low-pressure limit, such that eq 16 is the appropriate form for the distribution function for internal energy and angular momentum. Under the assumption of transition state theory, the complex subsequently dissociates back to reactants or forms the substitution products in an irreversible process. In this way, the efficiency of the bimolecular reaction ($k_{\text{exp}}/k_{\text{coll}}$) can be related to the ratio of the thermally averaged unimolecular rate constants

for dissociation of the reactants complex by eq 10. The optimal value of ΔH^\ddagger is then determined by comparison of the experimental efficiency with the calculated efficiencies for a series of values of ΔH^\ddagger .

Branching Ratios and KERDS. Metastable branching ratios were calculated with eq 21, for the fraction of dissociation into channel i for an ion with n dissociation channels. The probability of dissociation in the experimental time window, $P_{\text{diss}}(E, J)$, is given by eq 20.

$$f_i = \frac{\int_0^\infty \int_0^{J_{\text{max}}} dE dJ P(E, J; T) P_{\text{diss}}(E, J) F_i(E + \Delta H_i, J)}{\sum_{i=1}^n \left(\int_0^\infty \int_0^{J_{\text{max}}} dE dJ P(E, J; T) P_{\text{diss}}(E, J) F_i(E + \Delta H_i, J) \right)} \quad (21)$$

Branching ratios were calculated for $P(E, J; T)$ given by eq 16 and eq 18. The quantity ΔH_i is defined as the 0 K heat of formation of the appropriate transition state, relative to the separated reactants, as in Figure 1.

The KERDs for metastable dissociation were calculated as described previously.^{12,41} Internal excitation of the products was modeled by assuming different values for the overall bimolecular reaction enthalpy. The optimal fit of the calculated KERDs to the experimental data was determined by a visual inspection of the data.

Supporting Information Available: Plots of metastable vs CAD experimental KERDs for eqs 2–4; **z**-matrixes with optimized geometries; tables of absolute energies from ab initio calculations; tables of calculated vibrational frequencies; tables of parameters for PST-ADO calculations (19 pages, print/PDF). See any current masthead page for ordering information and Web access instructions.

JA9730775